JCTC Journal of Chemical Theory and Computation

Article

pubs.acs.org/JCTC

Multiscale Simulation of Liquid Water Using a Four-to-One Mapping for Coarse-Graining

Anu Nagarajan,[†] Christoph Junghans,[‡] and Silvina Matysiak*,[†]

[†]Fischell Department of Bioengineering, University of Maryland, College Park, Maryland 20742, United States

[‡]Theoretical Division, Los Alamos National Laboratory, Los Alamos, New Mexico 87545, United States

Supporting Information

ABSTRACT: We present a multiresolution simulation scheme for the solvent environment where four atomistic water molecules are mapped onto one coarse-grained bead. Soft restraining potentials are used to allow a resolution exchange of four water molecules into a single coarse-grained site. We first study the effect of adding restraining potentials in liquid water using full all-atom simulations. The usage of very soft restraining potentials to bundle four nearest neighbor water molecules does not disrupt the hydrogen bonding patterns in the liquid water. The structural properties of the first solvation shell around hydrophobic, hydrophilic, and ionic solutes are well preserved when soft restraining potentials are added. By modeling a bundle of four water molecules as a single molecule, a smooth transition and free exchange between coarse-grained and all-atom resolution is possible by using the adaptive resolution scheme (AdResS).

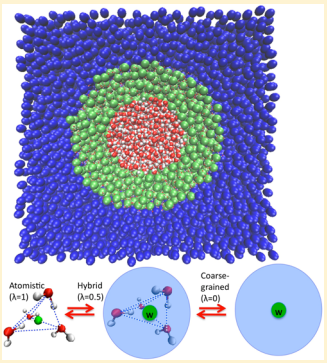

1. INTRODUCTION

Molecular dynamics simulations of biological macromolecules have provided many insights about the internal motions of these systems for over 35 years. Starting from a very short simulation of 9.2 ps of BPTI in a vacuum in 1977,[1] major computational advancement in recent years has enabled exploration of systems on the microsecond time scale.[2,3] The gains of greater computational power are used in studying larger and more complex systems.[4−6] One of the major challenges that the molecular dynamics community faces today is the ability to access long time scales for large protein systems, which is critical to characterize protein function. This computational inaccessibility partly comes from the requirement of an accurate description of the aqueous environment that is important to biomolecular simulations.[7−10] To fulfill this requirement, even for a medium-sized protein, thousands of explicit water molecules need to be placed in its vicinity. The computational cost of simulating these extra thousands of water molecules far exceeds that of simulating the protein alone. Sampling through the possible conformations of proteins already presents a computer intensive calculation but the enormous challenge in studying these properties is the size of the system due to the representation of the aqueous environment. Achieving longer time scales in all-atom simulations of proteins is critical to computationally characterize protein function.

One way to overcome this challenge is to use the implicit or continuum solvent models[11−13] where the bulk solvent is represented as a continuous region with a dielectric constant. This method helps overcome the need for explicit representation of the solvent but has its disadvantages as well. A consequence of the approximations involved in the implicit representation of the solvent is that the energy landscape in the vicinity of the protein is altered and may cause structural distortions.[14,15] Ideally, explicit representation of the solvent through atomistic simulations gives us accurate insights about the properties and interactions in the system,[16,17] but the computational cost of simulating big systems with explicit solvation is very high, and accessing longer time scales becomes challenging. Coarse-grained models[18−20] are an attractive alternative to explicit models, allowing for simulations of larger systems and longer time scales, while still providing realistic structural details.[21−24] The most common approach encompasses the removal of nonrelevant degrees of freedom from the simulated system. As a consequence of reducing the number of interaction sites in the system upon coarse-graining, the trajectories calculated with these types of models are several orders of magnitude faster than all-atom models. However, the main drawback of coarse-grained approaches lies in the lack of an atomistically detailed description.[25,26]

Multiscale modeling techniques aim to bridge the gap between the microscopic and mesoscopic time and length scales.[27−30] In these techniques, different levels of theory are combined to describe a system at varying scales or resolutions. Multiscale methods can be classified as serial or parallel depending on if the different resolutions interact with each other or not.[27,30]

In all-atom/coarse-grained parallel multiscale methods, the all-atom and coarse-grained representations of the systems are modeled concurrently.[31,32,28,30,33−35] These methods combine all-atom models of a given subsystem with coarse-grained

Received: July 1, 2013
Published: October 8, 2013

representations characterized by adaptive or rigid boundaries. High- and low-resolution models directly interact in these approaches. In particular, the adaptive resolution scheme (AdResS)[31,36−38] allows one to interface regions with different molecular representations while maintaining a free exchange of particles and equilibrium between resolutions. Recently, some of us have applied this approach to simulate liquid water with two resolutions using a one-to-one mapping[36,39] (one water molecule:one coarse-grained bead) and to solvate hydrophobic solutes.[37]

Increasing the mapping from one-to-one to "n water" molecules to a single coarse-grained bead will reduce the number of interaction sites in the system and thus enable us to achieve longer time scales. The mapping of several small molecules into a single coarse-grained site brings new challenges in adaptive resolution simulations. Since all-atom water molecules diffuse too far away, "on-the-fly" bundling and mapping of nearest neighbor water molecules is computationally expensive and challenging. The key methodological issue in implementing the AdResS approach with an "n water molecule": one CG bead is how to do the mapping. We have chosen to restrain the motion of water molecules within a cluster of "n water" molecules in the atomistic region.[40] To avoid introducing artifacts into the hydrogen bonding network of liquid water, it is desirable that the bundles can keep the nearest neighbor water structure tetrahedral, which can be achieved by using three to five water molecules. This would enable water molecules to exist in the atomistic representation, but because they are bundled together, the mapping to a coarse-grained bead becomes much simpler. We have chosen the four-to-one mapping in the present work since many coarse-grained models of proteins and lipids with explicit solvation use such mapping scheme,[41,42] and it has been shown to have the optimal balance between computational efficiency and accurate solvation properties.[64]

In this paper, we first discuss the addition of very soft restraining potentials to constrain the relative motion of four water molecules within a bundle. We then examine the effect of bundling in the structural and solvation properties of the solvent. In particular, we present a comparison of the ion, hydrophobic and hydrophobic hydration properties with and without the addition of soft restraining potentials. We then present the results of the adaptive resolution simulation of liquid water using a four-to-one mapping. Finally, we present the main conclusions as well as possible extensions of the method and these studies.

2. METHODS

2.1. Multiscale Simulation. For the multiscale simulation, GROMACS version 4.6[43] with AdResS implementation was used.[37,39] This method allows for smooth coupling and interchange between different degrees of resolutions. A water box is spatially partitioned with two resolutions, all-atom and coarse-grained as depicted in Figure 1a, using a spherical geometry for the atomistic region. The small region with higher resolution (atomistic) is coupled to a low-resolution model (coarse-grained) by the introduction of a hybrid region. This transition region contains hybrid molecules that are composed of a bundled water molecule with an additional center-of-mass virtual site (see Figure 1b) that serves as an interaction site (green region). This transition region allows the particles to change their resolution from atomistic to coarse-grained and vice versa. The smooth transition in resolution is achieved by a

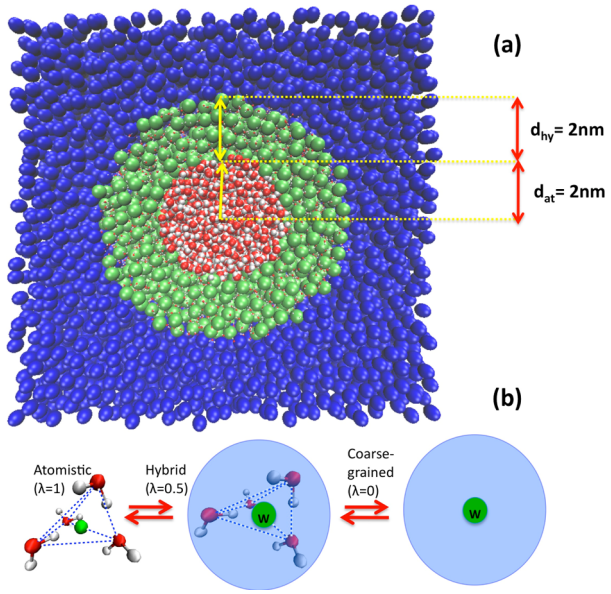

Figure 1. (a) Snapshot of the multiscale system. The central sphere is the atomistic region with radius = 2 nm. The region between two concentric shells with radii of 2 and 4 nm serves as the hybrid region (green). The rest of the system (blue) is in coarse-grained representation. (b) The coarse-grained molecules are represented at the right and the all-atom water bundle at the left. The middle hybrid molecule interpolates between the two. Individual water bundles in atomistic resolution are held together by soft restraints (dotted lines). Each molecule has a virtual site at its center of mass for easy mapping to a coarse-grained bead.

weighting function that allows for mixing of forces between the two regimes. The weighting function $\lambda = 1$ corresponds to the atomistic region, and $\lambda = 0$ corresponds to the coarse-grained region. Any value in between corresponds to the interface region. A molecule in the atomistic region is defined as the four water molecules that belong to a bundle as seen in Figure 1b. The forces acting between the center of mass of molecules α and β is given as

$$F_{\alpha\beta} = \lambda(X_\alpha)\lambda(X_\beta)F_{\alpha\beta}^{\text{atom}} + [1 - \lambda(X_\alpha)\lambda(X_\beta)]F_{\alpha\beta}^{\text{cg}} \quad (1)$$

where $F_{\alpha\beta}^{\text{atom}}$ is the sum of all intermolecular atom interactions between explicit atoms of the molecules α and β, and $F_{\alpha\beta}^{\text{cg}}$ is the sum of all coarse-grained intermolecular interactions. $\lambda(r)$ is a function of the center of mass and goes smoothly from 1 (atomistic) to 0 (coarse-grained).[36] Water molecules will have different resolutions depending on the distance to the center of the all-atom region. By this choice of interactions, the hybrid and all-atom molecules interact with molecules in the coarse-grained region on a coarse-grained level. The coarse-grained particles "see" the fully atomistically resolved bundles as coarse-grained molecules. On the other hand, the interactions of the hybrid molecules with the molecules in the explicit region will be a combination of explicit−explicit and CG−CG interactions to smoothly and efficiently equilibrate additional degrees of freedom upon moving toward the explicit regime.

2.2. Virtual Sites Construction. The center of mass of the four water molecules which are restrained by soft potentials act as the mapping points for the coarse-grained beads in the multiresolution simulation. The virtual site is located on the center of mass of the bundled water molecule. The virtual site does not have any mass or charge.

2.3. Coarse-Graining of Bundled Water. A single-site isotropic coarse-grained potential was obtained by matching the corresponding center of mass distribution function of a bundled water system using the inverse Boltzmann method with the VOTCA package.[44,45] The coarse-grained interaction potentials are centered on the center of mass of a water bundle. We performed 283 iterations of Inverse Boltzmann,[46] each iteration of 0.5 ns length. The effective potential was set to zero after 2 nm, which is well beyond the second hydration shell in the radial distribution function.

2.4. Thermodynamic Force. The hybrid region where the force interpolation is applied is known to lead to artifacts in density.[32] Recently, the thermodynamic force (TF) method was used to correct for density anomalies in the hybrid region.[39] The density artifacts can be fixed by applying a thermodynamic force in the hybrid region on the center of mass of the molecules. The force can be computed from the changes in chemical potential in the all-atom and coarse-grained region. The force correction in each step is obtained using eq 2:

$$F_{th}^{i+1}(r) = F_{th}^{i}(r) - \frac{M_{\mathrm{BundledWater}}}{\rho_0^2 \kappa_T^{at}} \nabla_r \rho(|r|) \tag{2}$$

where ρ_i is the normalized radial density from the center of the all-atom region and κ_T^{at} is the isothermal compressibility of the all-atom region. The region where thermodynamic force was applied was extended by 0.2 nm into both the all-atom and the coarse-grained zones.

3. SIMULATION DETAILS

3.1. Atomistic Simulations. The molecular dynamics simulations described in this work were performed using the GROMACS software package.[43] Version 4.5.4 was used for atomistic simulations of bundled water and unrestrained SPC water.[47] For all simulations, a time step of 0.1 fs was used. Twin-range cutoff was used to compute the nonbonded interactions. Coloumb and Lennard-Jones interactions were computed within 0.9 nm at every time step. Interactions beyond 0.9 nm but within 1.4 nm were computed with every update of the neighbor list, which was every 10 steps. The reaction field correction[48] with a dielectric constant of 80.0 was used beyond the 1.4 nm cutoff distance. For the atomistic simulations, a Berendsen thermostat[49] with a time constant of 0.1 ps and a reference temperature of 323 was used. The Berendsen isotropic pressure coupling[49] was used with a compressibility of 4.5 e−4 bar^{-1}, a reference pressure of 1 bar, and a coupling constant of 0.3 ps. For the atomistic bundled water simulation, a cubic box with 262 bundled water molecules, which is equivalent to 1048 SPC water molecules, was used. The water geometry was constrained using the SETTLE algorithm.[50] For the free unrestrained SPC water[51] simulation, 216 SPC water molecules in a cubic box were used. All the simulations were run for 100 ns.

3.2. Adaptive Resolution Simulation. We started the adaptive resolution simulation with an equilibrated water box (13.5 nm^3) with 17 753 bundled water molecules. The simulation was run for 20 ns in constant volume with a reference temperature of 323 K. The reaction field correction was applied with a dielectric constant of 80.0 beyond the 1.4 nm cutoff distance. We used a spherical geometry for the adaptive resolution simulation, where the atomistic region is a sphere of radius d_{at} = 2 nm and the hybrid width d_{hy} = 2 nm (as seen in Figure 1a). TF was applied from 1.8 to 4.2 nm to correct for the density artifact in this region. Please refer to the VOTCA manual page for the details. The TF simulation was run for 191 iterations with each iteration run for 0.1 ns. A Langevin thermostat[52] was employed to remove or supply the latent heat caused by the switch of resolutions.

4. RESULTS

4.1. Parameterization of the Bundled Water Model. In order to bundle four atomistic water molecules together, we use a soft harmonic potential between oxygen atoms of the water molecules as depicted in Figure 1b. We tested our model with different force constants and equilibrium distances between oxygen atoms and compare the radial distribution function (rdf) of oxygen atoms with that of the unrestrained SPC water model[51] (Figure S1a−e, Supporting Information). Although all of them reproduced the peak of the first hydration shell well (at around 0.3 nm), we observed that higher force constants created a larger depletion region after the first hydration shell, which encroaches into the second hydration shell, when compared with unrestrained SPC water. On the other hand, smaller equilibrium distances between oxygen shifts the depletion region after the first hydration shell, in addition to decreasing the density in the depletion region. In other words, lowering the equilibrium distance makes the depletion more than that of unrestrained SPC water.

We find that the force constant of 400 kJ mol^{-1} nm^{-2} with an equilibrium distance of 0.35 nm gives the most agreeable radial distribution of oxygen−oxygen atoms. We also explored the density of water as it varies with force constant and equilibrium distances (Table ST1, Supporting Information). We find that a lower equilibrium distance shifts the density to a higher value since the water molecules are closer together than usual. This trend is observed with all the force constants. As the force constants for the restraining potentials are increased, this in turn also increases the density of water. We find that a force constant of 400 kJ mol^{-1} nm^{-2} with an equilibrium distance of 0.35 nm gives the most agreeable density of 990.68 kg m^{-3} for bundled water and radial distribution of oxygen−oxygen atoms, which is very close to that of unrestrained SPC water.

Further, when we compared the rdf of C-alpha atoms of alanine dipeptide and oxygen atoms of water molecules, we found that the bundled water with a force constant of 400 kJ mol^{-1} nm^{-2} and equilibrium distance of 0.35 nm gives the closest agreement with unrestrained SPC water (Figure S3).

4.2. Effects of Bundling in Bulk Water Properties. We further characterize the structural properties of liquid water using the optimized bundled water model and compare them with the unrestrained SPC model. The rdf of oxygen and hydrogen atoms also shows very good correlation between the bundled water and free SPC water (Figure 5b). Our bundled water model captures the location of the oxygen and hydrogen atoms close to that of the free SPC water. In order to more thoroughly quantify the structural properties of our model, which are not completely defined by the rdf, we computed the orientational order parameter (q),[53,54] which provides information about the tetrahedrality of the network of water around a particular water molecule. A value of 0 represents a random orientation, and a value of 1 represents a perfect tetrahedral orientation. The bundled water exhibits a q of 0.67 ± 0.18, which deviates slightly from the unrestrained model (q = 0.63) but is in excellent agreement with the TIP5P and TIP4P water models (0.65−0.68).[55] Another feature to note

about the rdf of the oxygen atoms of bundled water model is that its shape is close to that of the TIP3P water model.[56] The flattened shape of the radial distribution of bundled water after the first maxima in the TIP3P model is also seen in our model.

To explore the effect of bundling in the electrostatic properties of bulk water, we have computed the dipole moment distribution of the bundle water and of the unrestrained SPC water taken from four nearest neighbor water molecules at a time. As shown in Figure S2a and b, the dipole moment distribution of the bundled water molecules has a peak at around 5.25D, while the distribution of dipole moment of the unrestrained system taken four water molecules at a time has a peak at a value of 5D.

It is expected that bundling will influence the diffusion of the water molecules since bundled water will have a higher hydrodynamic radius. To compare the effects of the restraining potential on the dynamical properties of water, we computed the diffusion coefficient using the Stokes−Einstein relation. We found the diffusion coefficient of bundled water to be $1.24 \pm 0.0376 \times 10^{-9}$ m^2 s^{-1} at 300 K. Unrestrained SPC water has a diffusion coefficient of $4.22 \pm 0.0928 \times 10^{-9}$ m^2 s^{-1} at 300 K, and the experimental value for water is 2.3×10^{-9} m^2 s^{-1} at 300 K.[61] Since the bundled water has to move as a tetramer, it is expected to have a lower diffusion coefficient compared to individual SPC water molecules. The diffusion coefficient of bundled water cannot be directly compared to that of unrestrained SPC water; rather a factor of 4 gives a more appropriate comparison. We also computed the thermodynamic properties like the coefficient of thermal expansion (unrestrained SPC water = 0.00014 K^{-1}, bundled water = 0.00038 K^{-1}, and experimental value = 0.000257 K^{-1} [62]), isothermal compressibility (unrestrained SPC = 1.99392 e−10 J m^{-3}, bundled water = 3.88065 e−10 J m^{-3}, and experimental value = 4.52 e−10 Pa^{-1} at 298 K[62,63]), and heat capacity Cp (unrestrained SPC = 96.525 J/(mol K), bundled water = 67.2561 J/(mol K), and experimental value = 75.312 J/mol K[62]). While properties of SPC water are known to deviate from the experimental values,[62] our bundled water model is closer to the experimental values of thermodynamic properties. Of course, these thermodynamic values have been measured per bundle, which consists of four water molecules.

4.3. Bundled Water with Alanine-Dipeptide and Phosphotyrosine-Binding (PTB) Domain. In order to assess the bundled water model and investigate the validity of the model with its interaction with protein molecules, we present the results from the simulations of alanine dipeptide and PTB domain (see Supporting Information) solvated with bundled water. We observe that for the PTB domain, the global RMS changes are the same in simulations with unrestrained SPC water and bundled water, although fast motions are not fully captured by the bundled water simulation (Figure S5a and b). For the structural properties of the hydration shell of the PTB domain, we considered only the surface residues that had a solvent accessible surface equal to 1 nm^2 or greater to characterize the hydration shell of solvent exposed residues.

The radial distribution function of the two protein systems' atoms with bundled water also provides information on the hydration properties of the bundled water as a solvent. Hydration water molecules interact closely with the protein,[9,10] and its properties are crucial because it contributes to protein stability, dynamics, and folding[7,8] and forms a network around the protein to keep it in solution. The radial distribution of hydrophobic atoms and the hydrophilic ones of alanine-dipeptide and the PTB domain with that of free SPC water show good agreement (Figure 2a and b for alanine dipeptide and Figure S6a and b for the PTB domain). The reason for a good agreement is that our model is very close in structure to the tetrahedral structure formed by free water at room temperature, and the hydrogen-bonded network is not disturbed. The individual water molecules inside the bundles are free to rotate and reorient according to the local environment.

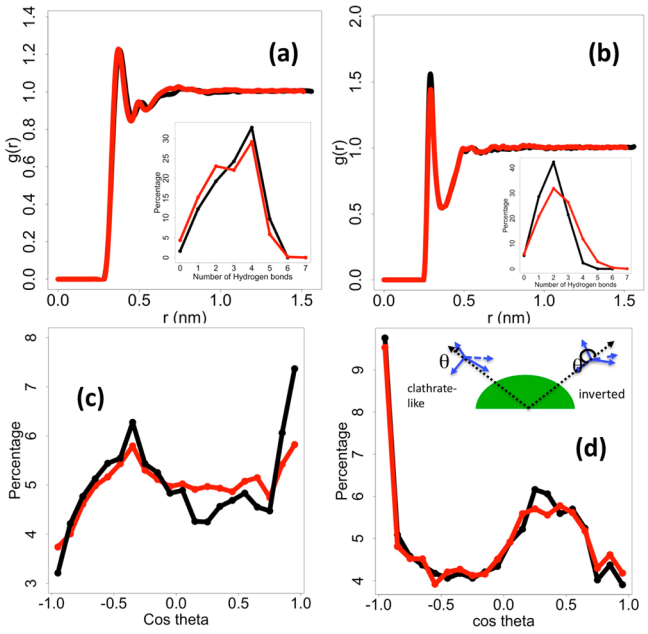

Figure 2. (a) The rdf of hydrophobic atoms of alanine-dipeptide and oxygen atoms in unrestrained SPC water (black) and bundled water (red). (Inset) Number of hydrogen bonds per water molecule around the hydrophobic atoms. (b) RDF of hydrophilic atoms of alanine dipeptide and oxygen atoms in unrestrained SPC water (black) and atomistic bundled water (red). (Inset) Number of hydrogen bonds per water molecule around the hydrophilic atoms. (c) The cos θ values for proximal water molecules around the hydrophobic atoms in unrestrained SPC water (black) and bundled water (red). (d) The cos θ values for proximal water molecules around the hydrophilic atoms in unrestrained SPC water (black) and bundled water (red). (Inset) Cartoon representation of clathrate-like and inverted orientation of water molecules around a solute.

We studied the hydrogen bonding patterns of water in the first hydration shell of hydrophobic and hydrophilic atoms of alanine-dipeptide and bulk water (Figure 2a and b insets) and also for the hydration shell of the solvent exposed residues of the PTB domain (Figure S7c and d). We see that water molecules around hydrophilic residues form fewer hydrogen bonds with the bulk water molecules in both water models. This is because water molecules can form hydrogen bonds with some of the hydrophilic atoms of the proteins. We see an opposite trend for the hydrophobic atoms, where water molecules surrounding those atoms make more hydrogen bonds with the bulk water. This is the case in both water models.

The solvent orientation around atoms of protein systems is shown in Figure 2c and d for alanine-dipeptide and Figure S7a and b for PTB protein. The individual water molecules proximal to each of the selected solute atoms are identified using the proximity analysis of Mehrotra and co-workers.[57] For

dx.doi.org/10.1021/ct400566j | J. Chem. Theory Comput. 2013, 9, 5168−5175

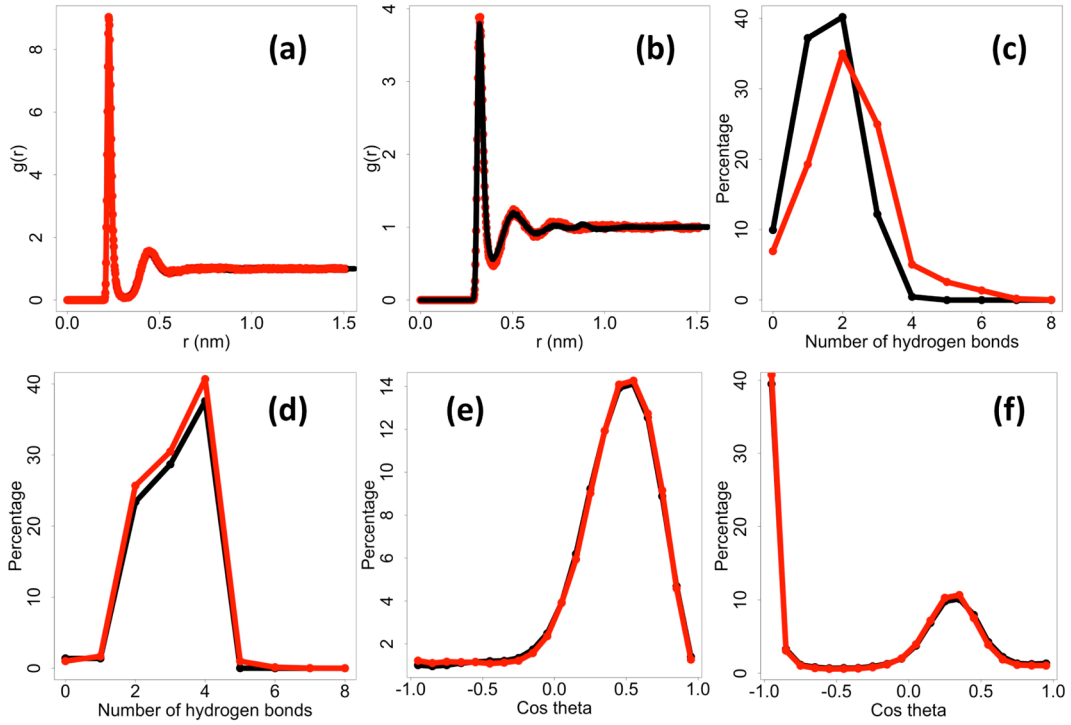

Figure 3. (a) rdf of Na^+ ion and oxygen atoms in unrestrained SPC water (black) and atomistic bundled water (red). (b) RDF of Cl^- ion and oxygen atoms in unrestrained SPC water (black) and bundled water (red). (c) Number of hydrogen bonds per water around the Na^+ ion in unrestrained SPC water (black) and bundled water (red). (d) Number of hydrogen bonds per water around the Cl^- ion in unrestrained SPC water (black) and bundled water (red). (e) The cos θ values for proximal water molecules around the Na^+ ion in unrestrained SPC water (black) and bundled water (red). (f) The cos θ values for proximal water molecules around the Cl^- ion in unrestrained SPC water (black) and bundled water (red).

hydrophobic atoms, water molecules orient themselves in a clathrate-like conformation (Figure 2d (inset)). The peaks at −0.33 and 1 represent this conformation. For hydrophilic atoms, water molecules adopt an inverted orientation pointing inward toward those atoms. This is because of hydrogen bond formation with alanine dipeptide. It is represented by the peaks at −1 and 0.33. This behavior of water molecules in the first hydration shell is consistent between both water models. This implies that the hydrogen-bonding network and orientational preference is not affected by the restraining potential and that our bundled water model captures the right structural properties of free SPC water.

To understand better the impact of bundled water on the free energy landscape of alanine dipeptide, we computed the free energy profile of alanine dipeptide and found them to be in close agreement with that obtained from simulation with unrestrained SPC water (Figure S4a and b). We find that bundling water molecules does not affect conformational preferences of alanine dipeptide since all the minima are captured well.

The bundling of water molecules will fall short in describing processes where there is an insertion of water molecules inside the core of a protein. Internal water mediated interactions are not expected to be captured with this model since four water molecules are bundled as one molecule. Processes like transport of individual water molecules through a membrane protein channel are not intended applications.

4.4. Solvation Structure of NaCl in Bundled Water. The changes in the solvation structure associated with a Na^+ and Cl^- ion pair in bundled and free SPC water has also been examined to fully characterize the impact of bundling in an ionic solvation structure. A distance restraint was imposed on the ion pair with a minimum distance of 0.8 nm and a maximum distance between the two ions to be 1 nm. The radial distributions of Na^+ and Cl^- ions are found to be in excellent agreement between the two models (Figure 3a and b). In order to study the hydrogen bonding pattern of the two models around the ions, we computed the number of hydrogen bonds per water molecule in the Na^+ and the Cl^- hydration shells (Figure 3c and d). We find the distribution of the two models in very good agreement with each other. Another structural property of water molecules we explored is the orientational preference. The distribution of angles the water molecules make with the surface normal of the ions for the two water models also shows very good agreement (Figure 3e and f). For Cl^- ions, the distribution of cos θ values shows a peak at −1 and 0.336. This is characteristic of an inverted orientation of water molecules around the ion. Whereas, the distribution of cos θ values for Na^+ ions shows a marked peak at 0.5, which corresponds to 60°. This implies multiple hydrogen bond donors interacting with the ion.

4.5. Multiscale Simulation of Liquid Water. In order to smoothly couple the atomistic bundled water and the CG resolutions, we use the AdResS scheme outlined in the Methods section. Large density fluctuations were observed during the 20 ns-long trajectory using the AdReS setup as seen in Figure 4. The coarse-grained potential derived from the inverse Boltzmann method ensures the correct rdf and compressibility.[58] The difference in chemical potential in the two regions produces a force that makes the molecules drift across boundaries leading to an inhomogeneous system.[39,59] To compensate for this force, we compute a counter thermodynamic force to be applied in the hybrid region of the system. The various iterations and the density fluctuations in the hybrid

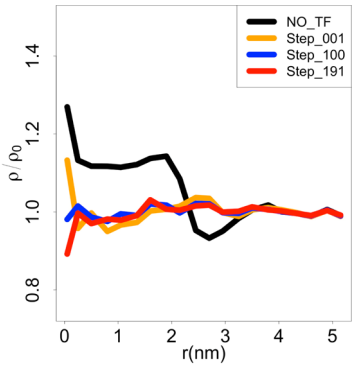

Figure 4. Density fluctuations in the simulations with and without TF for different iterations. The *x* axis is distance in nanometers, which represents the distance from the center of the atomistic region. The *y* axis represents the ratio of local density to bulk density.

region can be seen in Figure 4. It can be seen that there are improvements in the initial runs, but the density profile gets more refined with the number of iterations, finally producing a flat profile.

Bundling four atomistic water molecules and mapping onto one coarse-grained bead reduces the computational time required to simulate large systems compared to fully atomistic or 1:1 mapping schemes. We observe a speed up of up to 12 times from the AdResS simulations compared to a fully atomistic system of similar size. A detailed comparison between the bulk explicit simulations with and without the restraining potential on oxygen atoms and the all-atom regime in our multiresolution setup proves that our approach does not alter the main structural properties of the water model studied when the density is corrected.

Figure 5a and b show that the structural properties of the explicit regime in the multiscale system are exactly the same as in bulk bundled water simulations. The same excellent agreement is found for the bundled water center-of-mass rdf from the bulk bundled water simulation and the explicit and CG regions of the multiscale system (Figure 5c). This shows that although the interactions between the individual water molecules of the bundles are turned off in the coarse-grained region, we are able to reproduce the correct radial distribution function based on the atomistic region.

The hydrogen bonding patterns are preserved in the explicit region of the multiresolution setting (Figure 6b). The

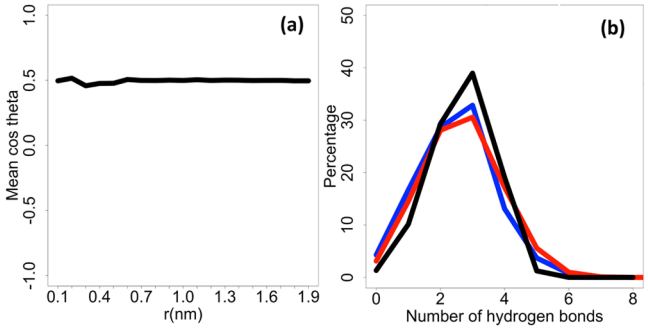

Figure 6. (a) Average cos θ values of water molecules in shells of radius r in the atomistic region of the multiscale simulation showing random orientation. (b) Number of hydrogen bonds per water molecule for unrestrained SPC water (black), bundled water in an atomistic simulation (red), and bundled water in a multiscale simulation (blue).

distribution of hydrogen bonds per water molecule almost coincides between bulk bundle water and the explicit region of the multiscale system. This is also consistent with the distribution of the number of hydrogen bonds of unrestrained SPC water.

Water molecules next to a neutral fluid surface reorient in a way that maximizes their hydrogen bonds.[60] As a consequence, the explicit molecules near the resolution interface could orient at the boundary as previously shown by some of the authors.[31,32] This effect can be avoided by using an appropriate interface layer. In the present work, we have used a conservative choice for the width of the interface layer of 2 nm, which is 2 times the length at which the water structure would be perturbed by a neutral surface.

Figure 6a shows the mean orientational parameter cos θ_{OH} (O−H vector and the radial direction of the atomistic region (refer Figure 1a)) as a function of distance from the center of the sphere (0,0,0). Bins of 0.1 nm are used. The hybrid region completely removes any orientational bias that could have been introduced in the explicit region by the coarse-grained region. The average orientation of the vectors can be quantified by the average cosine value. A mean cos θ_{OH} of 0.5 means random

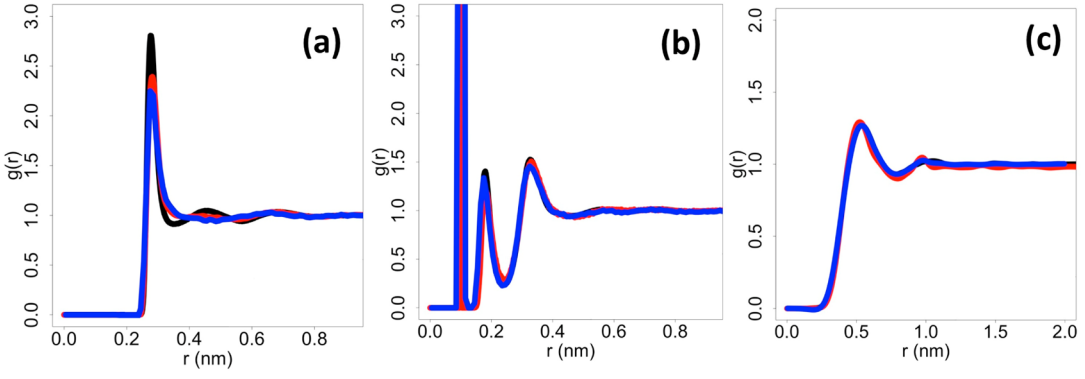

Figure 5. Bundled water in the atomistic region of the multiscale simulation is represented in blue. Bundled water in fully atomistic simulation is represented in red. Unrestrained SPC water in fully atomistic simulation is represented in black. (a) rdf of oxygen atoms. (b) rdf of oxygen−hydrogen atoms. (c) Center of mass of the bundled water molecule. The blue curve shows the bundled water in the atomistic region of the multiscale simulation. In red is the bundled water in fully atomistic simulation. In black is the coarse-grained bead in multiscale simulation.

dx.doi.org/10.1021/ct400566j | J. Chem. Theory Comput. 2013, 9, 5168−5175

orientation. Clearly, the hybrid region neutralizes the interface effect of the coarse-grained liquid water, and the bundle water molecules have fully equilibrated orientational degrees of freedom where they enter the explicit regime.

5. CONCLUSIONS

In this paper, we address the challenges faced in terms of simulation of liquid water when four-to-one mapping is used for coarse-graining. We present an approach to bundle water for multiresolution simulations. Bundling is crucial in multiresolution simulations when different resolutions are represented in parallel, because it ensures effective and easy mapping of the atomistic water to a coarse-grained water bead. The usage of very soft restraining potentials to bundle four nearest neighbor water molecules does not disrupt the hydrogen bonding patterns in the liquid water. The radial distribution function shows good correlation between the bundled and free water. The structural properties of the first solvation shell around hydrophobic, hydrophilic, and ionic solutes are well preserved when soft restraining potentials are added. In addition, bundling of liquid water does not disrupt the conformations explored by alanine-dipeptide. The bundled water model clearly mimics the hydrogen bond network of the reference unrestrained SPC model. Within a bundle, each water molecule can adjust its position and orientation depending on the local environment, thus capturing the correct signatures of hydrophobic, hydrophilic, and ion hydration. The thermodynamic properties like isothermal compressibility, coefficient of thermal expansion, and heat capacity are in good agreement with unrestrained SPC water and in even better agreement with experimental results. The dielectric constant also agrees well between the two models. The diffusion constant on the other hand was not expected to be the same between the two models since the bundles consists of four water molecules. By modeling each bundle as a single molecule, a smooth transition and free exchange between coarse-grained and all-atom resolution is possible. The presented multiscale approach can be easily applied to different mapping schemes. Future work will focus on incorporating polarization effects in the coarse-grained region of the multiresolution solvent to retain an accurate description of long-range interactions, which are critical to model solvation effects of ions and biomolecules. Work along these lines is currently being pursued in the lab.

■ ASSOCIATED CONTENT

Ⓢ Supporting Information

Additional results, figures, and tables. This material is available free of charge via the Internet at http://pubs.acs.org.

■ AUTHOR INFORMATION

Corresponding Author

*E-mail: matysiak@umd.edu.

Notes

The authors declare no competing financial interest.

■ ACKNOWLEDGMENTS

This research was supported in part by the National Science Foundation through XSEDE resources provided by The Texas Advanced Computing Center (TACC) under grant numbers [TG-MCB110075] and [TG-MCB120045]. We would also like to thank Sebastian Fritsch for his help and support with AdResS and the VOTCA package. Christoph Junghans thanks LANL for a Director's fellowship.

■ REFERENCES

(1) Mccammon, J. A.; Gelin, B. R.; Karplus, M. *Nature* **1977**, *267*, 585−590.
(2) Sorin, E. J.; Rhee, Y. M.; Pande, V. S. *Biophys. J.* **2005**, *88*, 2516−2524.
(3) Shaw, D. E.; Maragakis, P.; Lindorff-Larsen, K.; Piana, S.; Dror, R. O.; Eastwood, M. P.; Bank, J. A.; Jumper, J. M.; Salmon, J. K.; Shan, Y. B.; Wriggers, W. *Science* **2010**, *330*, 341−346.
(4) Kitao, A.; Yonekura, K.; Maki-Yonekura, S.; Samatey, F. A.; Imada, K.; Namba, K.; Go, N. *Proc. Natl. Acad. Sci. U. S. A.* **2006**, *103*, 4894−4899.
(5) Sanbonmatsu, K. Y.; Tung, C. *J. Struct. Biol.* **2007**, *157*, 470−480.
(6) Arkhipov, A.; Freddolino, P. L.; Schulten, K. *Structure* **2006**, *14*, 1767−1777.
(7) Raschke, T. *Curr. Opin. Struct. Biol.* **2006**, *16*, 152−159.
(8) Rupley, J.; Careri, G. *Adv. Protein Chem.* **1991**, *41*, 37−172.
(9) Higo, J.; Nakasako, M. *J. Comput. Chem.* **2002**, *23*, 1323−1336.
(10) Nakasako, M. *J. Mol. Biol.* **1999**, *289*, 547−564.
(11) Roux, B.; Simonson, T. *Biophys. Chem.* **1999**, *78*, 1−20.
(12) Feig, M.; Im, W.; Brooks, C. L. *J. Chem. Phys.* **2004**, *120*, 903−911.
(13) Koehl, P. *Curr. Opin. Struct. Biol.* **2006**, *16*, 142−151.
(14) Zhou, R. H.; Berne, B. J. *Proc. Natl. Acad. Sci. U. S. A.* **2002**, *99*, 12777−12782.
(15) Olson, M. A. *Proteins* **2004**, *57*, 645−650.
(16) Klepeis, J. L.; Lindorff-Larsen, K.; Dror, R. O.; Shaw, D. E. *Curr. Opin. Struct. Biol.* **2009**, *19*, 120−127.
(17) Levy, R.; Gallicchio, E. *Annu. Rev. Phys. Chem.* **1998**, *49*, 531−567.
(18) Clementi, C. *Curr. Opin. Struct. Biol.* **2008**, *18*, 10−15.
(19) Head-Gordon, T.; Brown, S. *Curr. Opin. Struct. Biol.* **2003**, *13*, 160−167.
(20) Shea, J.; Brooks, C. *Annu. Rev. Phys. Chem.* **2001**, *52*, 499−535.
(21) Trylska, J.; Tozzini, V.; Chang, C. A.; McCammon, J. A. *Biophys. J.* **2007**, *92*, 4179−4187.
(22) Sengupta, D.; Rampioni, A.; Marrink, S. *Mol. Membr. Biol.* **2009**, *26*, 422−434.
(23) Clementi, C.; Nymeyer, H.; Onuchic, J. N. *J. Mol. Biol.* **2000**, *298*, 937−953.
(24) Matysiak, S.; Clementi, C. *J. Mol. Biol.* **2006**, *363*, 297−308.
(25) Cascella, M.; Dal Peraro, M. *Chimia* **2009**, *63*, 14−18.
(26) Cascella, M.; Neri, M. A.; Carloni, P.; Dal Peraro, M. *J. Chem. Theory Comput.* **2008**, *4*, 1378−1385.
(27) Nielsen, S. O.; Bulo, R. E.; Moore, P. B.; Ensing, B. *Phys. Chem. Chem. Phys.* **2010**, *12*, 12401−12414.
(28) Praprotnik, M.; Delle Site, L.; Kremer, K. *Annu. Rev. Phys. Chem.* **2008**, *59*, 545−571.
(29) Peter, C.; Kremer, K. *Soft Matter* **2009**, *5*, 4357−4366.
(30) Ayton, G. S.; Noid, W. G.; Voth, G. A. *Curr. Opin. Struct. Biol.* **2007**, *17*, 192−198.
(31) Praprotnik, M.; Matysiak, S.; Delle Site, L.; Kremer, K.; Clementi, C. *J. Phys.: Condens. Matter* **2009**, *21*, 499801.
(32) Matysiak, S.; Clementi, C.; Praprotnik, M.; Kremer, K.; Delle Site, L. *J. Chem. Phys.* **2008**, *128*, 024503.
(33) Praprotnik, M.; Delle Site, L.; Kremer, K. *J. Chem. Phys.* **2005**, *123*, 224106.
(34) Noid, W. G.; Chu, J.; Ayton, G. S.; Krishna, V.; Izvekov, S.; Voth, G. A.; Das, A.; Andersen, H. C. *J. Chem. Phys.* **2008**, *128*, 244114.
(35) Christen, M.; van Gunsteren, W. *J. Chem. Phys.* **2006**, *124*, 154106.
(36) Praprotnik, M.; Matysiak, S.; Delle Site, L.; Kremer, K.; Clementi, C. *J. Phys.: Condens. Matter* **2007**, *19*, 292201.
(37) Fritsch, S.; Junghans, C.; Kremer, K. *J. Chem. Theory Comput.* **2012**, *8*, 398−403.

(38) Junghans, C.; Poblete, S. *Comput. Phys. Commun.* **2010**, *181*, 1447−1452.
(39) Fritsch, S.; Poblete, S.; Junghans, C.; Ciccotti, G.; Delle Site, L.; Kremer, K. *Phys. Rev. Lett.* **2012**, *108*, 170602.
(40) Fuhrmans, M.; Sanders, B. P.; Marrink, S.; de Vries, A. H. *Theor. Chem. Acc.* **2010**, *125*, 335−344.
(41) Nielsen, S. O.; Lopez, C. F.; Srinivas, G.; Klein, M. L. *J. Phys.: Condens. Matter* **2004**, *16*, R481−R512.
(42) Yesylevskyy, S. O.; Schafer, L. V.; Sengupta, D.; Marrink, S. J. *Plos Comp. Biol.* **2010**, *6*, e1000810.
(43) Hess, B.; Kutzner, C.; van der Spoel, D.; Lindahl, E. *J. Chem. Theory Comput.* **2008**, *4*, 435−447.
(44) Ruehle, V.; Junghans, C.; Lukyanov, A.; Kremer, K.; Andrienko, D. *J. Chem. Theory Comput.* **2009**, *5*, 3211−3223.
(45) Ruehle, V.; Junghans, C. *Macromol. Theory Simul.* **2011**, *20*, 472−477.
(46) Tschop, W.; Kremer, K.; Batoulis, J.; Burger, T.; Hahn, O. *Acta Polym.* **1998**, *49*, 61−74.
(47) Van der Spoel, D.; Lindahl, E.; Hess, B.; Groenhof, G.; Mark, A.; Berendsen, H. *J. Comput. Chem.* **2005**, *26*, 1701−1718.
(48) Tironi, I. G.; Sperb, R.; Smith, P. E.; Vangunsteren, W. F. *J. Chem. Phys.* **1995**, *102*, 5451−5459.
(49) Berendsen, H.; Postma, J.; Vangunsteren, W.; Dinola, A.; Haak, J. *J. Chem. Phys.* **1984**, *81*, 3684−3690.
(50) Miyamoto, S.; Kollman, P. *J. Comput. Chem.* **1992**, *13*, 952−962.
(51) Berendsen, H. J. C.; Grigera, J. R.; Straatsma, T. P. *J. Phys. Chem.* **1987**, *91*, 6269−6271.
(52) Adelman, S. A.; Doll, J. D. *J. Chem. Phys.* **1976**, *64*, 2375−2388.
(53) Errington, J. R.; Debenedetti, P. G. *Nature* **2001**, *409*, 318−321.
(54) Chau, P. L.; Hardwick, A. J. *Mol. Phys.* **1998**, *93*, 511−518.
(55) Jhon, Y. I.; No, K. T.; Jhon, M. S. *J. Phys. Chem. B* **2007**, *111*, 9897−9899.
(56) Jorgensen, W.; Chandrasekhar, J.; Madura, J.; Impey, R.; Klein, M. *J. Chem. Phys.* **1983**, *79*, 926−935.
(57) Mezei, M.; Mehrotra, P. K.; Beveridge, D. L. *J. Am. Chem. Soc.* **1985**, *107*, 2239−2245.
(58) Hansen, J. P.; McDonald, I. R. In *In Theory of Simple Liquids*; Academic Press: New York, 2006.
(59) Izvekov, S.; Voth, G. A. *J. Chem. Phys.* **2005**, *123*, 134105.
(60) Jedlovszky, P.; Vincze, A.; Horvai, G. *Phys. Chem. Chem. Phys.* **2004**, *6*, 1874−1879.
(61) Krynicki, K.; Green, C. D.; Sawyer, D. W. *Faraday Discuss. Chem. Soc.* **1978**, *66*, 199−208.
(62) Jorgensen, W. L.; Jenson, C. *J. Comput. Chem.* **1998**, *19*, 1179−1186.
(63) Fine, R. A.; Millero, F. J. *J. Chem. Phys.* **1973**, *59*, 5529−5537.
(64) Hadley, K. R.; McCabe, C. *J. Phys. Chem. B* **2010**, *114*, 4590−4599.